Volume 24
Number 43
21 November 2022
Pages 7507–7689

CrystEngComm

rsc.li/crystengcomm

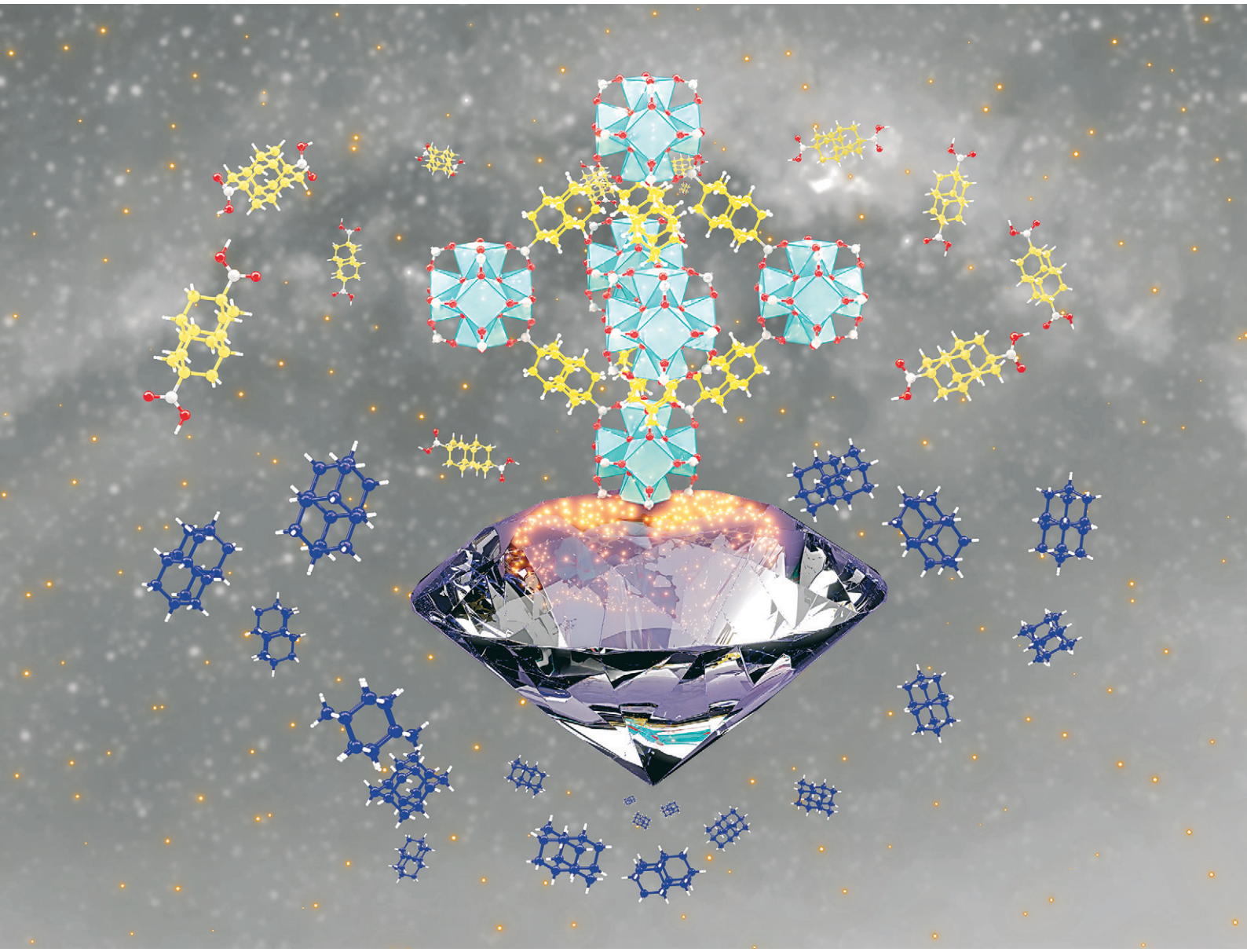

ISSN 1466-8033

ROYAL SOCIETY OF CHEMISTRY

COMMUNICATION

Ishtvan Boldog, Christoph Janiak *et al.*

A diamantane-4,9-dicarboxylate based UiO-66 analogue: challenging larger hydrocarbon cage platforms

CrystEngComm

ROYAL SOCIETY OF CHEMISTRY

COMMUNICATION

View Article Online
View Journal | View Issue

Cite this: *CrystEngComm*, 2022, **24**, 7530

Received 25th August 2022,
Accepted 23rd September 2022

DOI: 10.1039/d2ce01170k

rsc.li/crystengcomm

A diamantane-4,9-dicarboxylate based UiO-66 analogue: challenging larger hydrocarbon cage platforms†

Vasily Gvilava, [a] Maximilian Vieten,[a] Robert Oestreich, [a] Dennis Woschko, [a] Moritz Steinert,[a] Ishtvan Boldog, *[a] Roman Bulánek, [b] Natalie A. Fokina,[c] Peter R. Schreiner [cd] and Christoph Janiak *[a]

The first use of a bulky barrel-shaped ligand is demonstrated in HHUD-3, with accessible porosity only feasible for a defect structure. With 35%+ missing linker defects and S_{BET} = 890 m^2g^{-1} (N_2), HHUD-3 features higher CH_4 but lower CO_2 and H_2 adsorption than UiO-66.

Metal–organic frameworks (MOFs) are porous crystalline coordination polymers/networks consisting of metal ions, typically multi-nuclear clusters and bridging organic ligands.[1,2] These materials of large and designable porosity reach uniquely large surface areas of up to 8 × 10^3 m^2g^{-1}.[2,3] Potential applications are gas storage and separation,[4] catalysis,[2,4] drug delivery,[5] sensing, and luminescence.[6]

UiO-Zr-MOFs with the general formula $[Zr_6O_4(OH)_4(L)_6]$ are based on paradigmatic hexanuclear $\{Zr_6(\mu_3\text{-}O)_4(\mu_3\text{-}OH)_4(RCOO)_{12}\}$ clusters[7,8] connected to 12 neighbors by dicarboxylate organic linkers (L) to form an fcu (fcc) network ($Fm\bar{3}m$ max. symmetry).[9,10] The high oxidation state of Zr(IV), high charge density and bond polarization result in relatively strong and inert Zr(IV) and carboxylate–O bonds[11] leading to significant hydrothermal stability[12] and even limited stability in acidic media.[9,13] UiO-66, based on the terephthalate ligand, is an archetypal zirconium MOF with a unique combination of properties. Those are the high surface area, formation-tolerance regarding the modification of the ligand, efficient post-synthetic ligand exchange[14] and post-synthetic modification[15] for derivatization, possibility to exercise control over defects and their use as catalytic and docking sites as well as means to improve the surface area and pore-accessibility.[16] With its unique properties, UiO-66 is a progenitor of a whole MOF family, which, in addition to Zr, also includes Hf- or Ce-based analogues.[17,18] Further representatives are based on various ligands such as acetylenedicarboxylate (Hf-HHU-1),[19] biphenyl-4,4′-dicarboxylate (UiO-67), terphenyl-4,4′-dicarboxylate (UiO-68)[9] and even longer ethynylene augmented ligands (PIZOF series),[20] demonstrating the particularly successful case of the reticular chemistry approach. UiO-66 analogues based on relatively short molecular cage-based ligands (Fig. 1), namely the recently introduced bicyclo[1.1.1]pentane-1,3-dicarboxylate,[21] bicyclo[2.2.2]octane-1,4-dicarboxylate (NU-403),[22] the targeted, but not formally reported cubane-1,4-dicarboxylate,[23,24] and the poorly characterized derivative of 1,12-*closo*-dicarbadodecaborane-1,12-dicarboxylate,[9] indicate further interesting possibilities for materials based on even larger cage-based ligands. The less polar barrel-shaped form of the ligand, lower polarity, low rotational barrier (the cage connected to the carboxylate could act as a molecular rotor[21]), and minimized propensity towards specific stacking interactions compared to ligands with aromatic cores

[a] *Institut für Anorganische Chemie und Strukturchemie, Heinrich-Heine-Universität Düsseldorf, D-40204 Düsseldorf, Germany. E-mail: janiak@uni-duesseldorf.de*
[b] *Department of Physical Chemistry, Faculty of Chemical Technology, University of Pardubice, Studentska 573, 532 10 Pardubice, Czech Republic*
[c] *Institute of Organic Chemistry, Justus Liebig University, Heinrich-Buff-Ring 17, 35392 Giessen, Germany*
[d] *Center for Materials Research (ZfM), Heinrich-Buff-Ring 16, 35392 Giessen, Germany*

† Electronic supplementary information (ESI) available: Additional notes concerning the synthesis, PXRD patterns, Rietveld refinement and structural analysis, IR spectra, TGA, and gas adsorption studies. CCDC 2102614. For ESI and crystallographic data in CIF or other electronic format see DOI: https://doi.org/10.1039/d2ce01170k

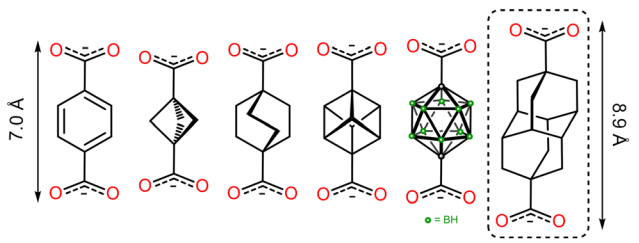

Fig. 1 Benzene-1,4-dicarboxylate compared to molecular cage-core dicarboxylate ligands based on bicyclopentane, cubane, bicyclooctane, 1,12-dicarba-*closo*-dodecaborane and diamantane (diamantane-4,9-dicarboxylate is shown in a dashed rectangle).

promise special adsorptive and separation (sieving) properties.

Diamantane is the second smallest representative of diamondoids or hydrogen terminated nanodiamonds,[25] which are rigid cage hydrocarbons with the highest thermodynamic stability among isomers.[26,27] They could be viewed as consisting of face-fused adamantane units having common six-membered rings (Fig. 1).[28] Adamantane ($C_{10}H_{16}$) is a well-known rigid tetrahedral molecular platform for supramolecular architectures, including MOFs.[29] Diamantane ($C_{14}H_{20}$) is composed of two adamantane cages and represents a linear building block upon functionalization at the axial bridge-head 4,9-positions (Fig. 1). Its use as a potential MOF-ligand platform is very limited with practically the only demonstrated case being the series of molybdenum oxide bis(triazol-4-yl)-4,9-diamantane coordination polymers.[30] From a small group of hydrocarbon cages occasionally used as a ligand platform, diamantane is arguably one of the longest and bulkiest barrel-shaped representatives to date, and- surprisingly no crystal structures of diamantane-4,9-dicarboxylic acid or its derivatives, particularly interesting for narrow-pore MOF design, were reported. What seemed like a straightforward and an easy transfer of synthesis conditions from paradigmatic MOFs based on linear ligands, like benzene-1,4-dicarboxylate or biphenyl-4,4′-dicarboxylate, proved to be a challenge, however. Notably, our attempts to prepare a MOF-5 analogue based on diamantane-4,9-dicarboxylate yielded alternative microcrystalline phases. Eventually, the synthesis of a UiO-66 analogue, seemingly less susceptible to steric hindrances, was successful, albeit not without difficulties regarding the quality and yield.

Here we report the synthesis, structure, and gas adsorption properties of a new UiO-66 analogue (in the following HHUD-3)‡ based on diamantane-4,9-dicarboxylate. The synthesis was carried out in sealed culture tubes using *N*,*N*-dimethylformamide (DMF) as the solvent and formic acid as the modulator (see Table S1, ESI†).§ Successful crystallization of the product depended on the use of a sufficiently high concentration of the ligand (otherwise, formation of gels was typically observed). The relatively poor solubility of the ligand made the range of optimal concentration relatively narrow. High ligand excess (molar ratio M : L = 3 : 8) ensured products of high crystallinity. However, when near 1 : 1 stoichiometric metal : ligand ratios were precisely observed, the reproducibility was sufficient. The optimal metal : linker ratio was found to be 7 : 8, which led to a product with the highest surface area (see Tables S1 and S5,† sample 1 *vs.* 2).

The small scale of the synthesis was found to be important. Attempts to scale up reaction sizes by a factor of three already led to a strong decrease in the crystallinity of the resulting product (the dependence of product quality on the synthesis scale is rather typical; *e.g.* for UiO-66, a decrease of specific surface area by ~1/3 upon ~×30 scale-up was documented).[12] In order to obtain the required amounts of the compound for further analyses, several small-sized batches of the same composition were run in parallel under identical conditions and the batches were combined.

The structure of the product, HHUD-3, obtained in the form of a microcrystalline powder with excellent crystallinity, was proven *via* Rietveld refinement of the PXRD data (Fig. 2 and S2;† the complete data set is presented in Table S2, ESI†).¶ An **fcu** structure model ($Fm\bar{3}m$, ligand disorder *via* inversion center, Fig. S7†), isostructural to the standard UiO-66,[16] was used (no fine low-angle pattern features characteristic of the regular **reo** structure were observed;[31] no signs of the **hcp** phase were noted as well).[32] The refinement significantly improves, when defects are represented by partially occupied diamantane moieties (a low precision number of ~1.4 missing linkers per cluster was refined).§

Thermogravimetric analysis (TGA) of HHUD-3, performed on an activated sample (140 °C, 10^{-3} Torr) also used for the gas adsorption measurements, shows only a minor weight loss below 200 °C (section S4, ESI†). The apparent decomposition starts slightly above 250 °C (Fig. S9, ESI†). From the TGA, 2.1+ missing-linker defects per Zr_6-formula unit were calculated as a low estimate (see section S4, ESI†), which is slightly higher than the ~2.0 defects in the most defective HCl-modulated UiO-66,[33] let alone the non-modulated and formic acid modulated cases of the latter.[34,35] Two missing linker defects are close to a realistic maximum of defects, with three defects being a theoretical maximum compatible with a 3D structure. The defect-free UiO-66 is thermally stable up to 450 °C in oxygen,[36] while the HCl modulated, defect-rich UiO-66 starts to decompose at slightly above 200 °C.[33] The low decomposition temperature of HHUD-3 based on a stable ligand is considered an indirect indication of the large number of defects.

The theoretical surface area based on the structural data was determined both for the defect-free network and for a

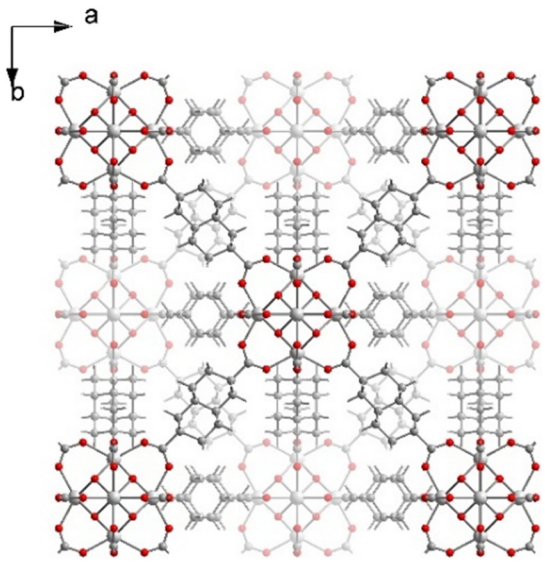

Fig. 2 The idealized non-disordered ($Fm\bar{3}$) presentation of the crystal structure of HHUD-3 (section S2, ESI†). Up to 4.4 out of 12 connections between the $[Zr_6(\mu_3\text{-}O)_4(\mu_3OH)_4]$ secondary building units (SBUs) are represented by missing linker defects.

model with two ordered missing linker defects in a form of a model **bcu** net (see section S5, ESI†). The total surface area of the defect-free compound was calculated to be 918 $m^2\ g^{-1}$, whereas the model with two defects would have 1854 $m^2\ g^{-1}$ (1.82 Å probe radius, equivalent to a N_2 molecule with 3.64 Å kinetic diameter). However, there is a stark difference between the accessible surface areas for the given probe size. For the model with two missing ligands per formula unit, the whole surface area is accessible, while for the defect-free model, there is no accessible surface area at all (the pores remain inaccessible for probe diameters larger than at least 2.4 Å).

The experimental determination of the porosity of HHUD-3 was performed by nitrogen (77 K) and argon (87 K) adsorption. The samples were activated to remove the solvents from the pores at 140 °C (it was proven that higher degassing temperatures did not influence significantly the measured surface areas; see Fig. S12, ESI†). The highest BET surface areas for HHUD-3 were found to be 869 $m^2\ g^{-1}$ based on N_2 sorption and 811 $m^2\ g^{-1}$ based on Ar sorption (gas sorption data for all samples are summarised in Table S5, ESI†), with a micropore volume of 0.244 $cm^3\ g^{-1}$ and 0.211 $cm^3\ g^{-1}$, respectively. Comparing these measured data with the theoretical calculations, the measured surface area of 869 $m^2\ g^{-1}$ is approximately in the middle between the non-porous case of the idealized defect-free compounds and 1854 $m^2\ g^{-1}$ for the compound with a near-maximal amount of ordered defects. This could partially be explained by the existence of non-accessible pores in the structure due to the uneven distribution of the missing linkers (for comparison: the calculated surface area for a defect-free UiO-66 model is 1145 $m^2\ g^{-1}$ *vs.* 1105 $m^2\ g^{-1}$ from experimental N_2 adsorption-based BET values for the defect-free UiO-66, and ~1250 $m^2\ g^{-1}$ for a typical[37] non-modulated UiO-66 material with a relatively low amount of defects).

Both the nitrogen and argon adsorption isotherms (Fig. 3) demonstrate a type I(b) behavior, indicating a generally microporous material with larger micropores (up to 2.0 nm pore diameter by definition) and possibly with an added share of small mesopores. The small hysteresis, close to an H3 type (narrow, uniform width; indicates broad pore size distribution), represents a textural effect of aggregated crystals.[38] The NLDFT pore size-distribution of HHUD-3 calculated from argon sorption shows the primary maxima of the pore size-distribution at 8 and 13 Å (Fig. S13, ESI†); the secondary maxima, corresponding to mesopores with diameters of ~3.5, 5, and 10 nm, are generally small in comparison. However, a minor variation of the conditions led to a variant of HHUD-3 with a strongly increased amount of mesopores with 3.5 nm diameter (sample 3 in Fig. S13, ESI†). This might indicate the presence of missing cluster defects. The sample also features a much wider hysteresis, rather suggesting the presence of large ink-bottle pores with narrow entrances, and generally demonstrating the strong dependence of the material's quality on synthetic conditions.

The CO_2, CH_4, and H_2 low-pressure adsorption isotherms are given in Fig. 4 (see Table S5 for the summary, including the actual uptakes at 0.96 bar, ESI†). The extrapolated adsorption values at 1 bar of different gases for HHUD-3 *vs.* reported values for UiO-66 are 1.90 mmol g^{-1} *vs.* 3.14 mmol g^{-1} (ref. 40) for CO_2 (273 K); 5.88 mmol g^{-1} (1.20 wt%) *vs.* 6.95 mmol g^{-1} (1.38 wt%)[39] for H_2 (77 K); 1.01 mmol g^{-1} *vs.* 0.84 mmol g^{-1} (ref. 40) for CH_4 (273 K). It is worth nothing that the uptake at low pressures (*i.e.* far from complete pore filling) is generally proportional to the surface area for similar compounds (this statement for H_2 is known as Chahine's rule[41,42]). As HHUD-3 has a lower surface area (by a factor of ~1.4), the lower adsorption of H_2 and CO_2 is in accordance with the expectations (even if the difference in the case of the former is small). In contrast, the higher

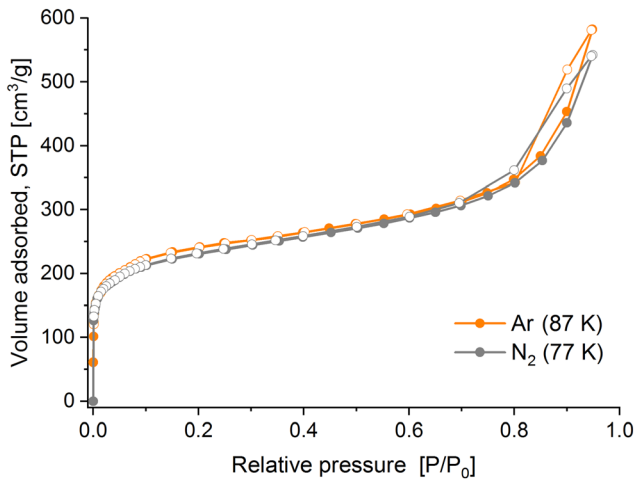

Fig. 3 N_2 and Ar adsorption isotherms for HHUD-3 (the adsorption branches are represented by filled symbols and the desorption branches by empty symbols).

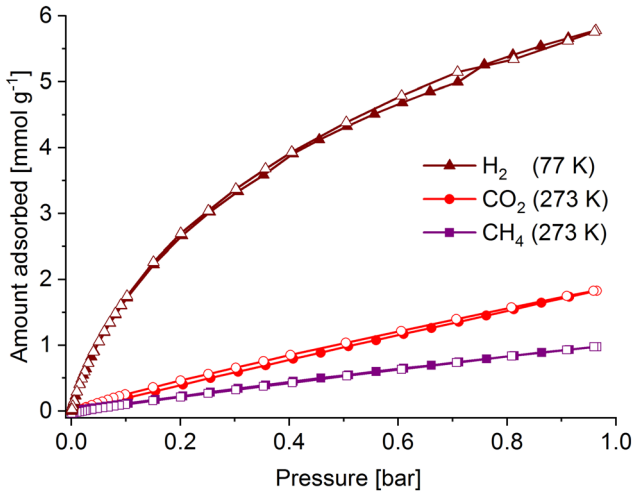

Fig. 4 H_2, CH_4, and CO_2 sorption isotherms for HHUD-3 (the adsorption branches are represented by filled symbols and the desorption branches by empty symbols).

adsorption of CH_4 by HHUD-3 is unexpected. In HHUD-3, the average polarity of the surface is significantly lower compared to that of UiO-66 (the metal-oxide clusters are better shielded by the sterics of the ligand, and a part of the surface of the diamantane also exceeds the benzene surface due to the larger size of the former). Lower polarity should mean in general weaker interactions and less specific adsorbent–adsorbate interactions. While confirmed for CO_2, the case of methane is different, with higher absolute amounts adsorbed. The plausible, yet somewhat speculative, explanation is that the suitably-shaped diamantane-lined pockets in HHUD-3 offer several CH···HC London dispersion[43] contacts for methane with a significant cumulative strength (a manifestation of the "like dissolve like" principle enhanced by good fitting of the molecular components). For example, the high vaporization enthalpies and melting points of polyhedranes (*e.g.* m.p. of ~450 °C for dodecahedrane) are attributed to the aggregate action of CH···HC contacts, named "sticky finger" interactions in this context.[44] Hence, HHUD-3 might interact even better with larger hydrocarbons and provide improved selectivity for different isomers.

In conclusion, an optimized synthesis of HHUD-3, a particular UiO-analogue based on a novel ligand with a barrel-shaped diamantane core, is reported together with structural characterization. Due to the shape of the ligand, the non-defective structure should apparently have been non-porous, however significant porosity was observed experimentally due to the high defect ratio. Optimal surface areas were reached in a relatively narrow range of synthetic conditions. Yet the porosity characteristics were exceedingly dependent on the experimental parameters, suggesting the importance of fine factors, which is in line with the expected strong dependence of the accessible surface area on defects. The clear relative preference towards adsorption of CH_4 *vs.* CO_2 and H_2 by HHUD-3 compared to UiO-66 together with a strong dependence of qualities on the defect rate makes HHUD-3 an excellent adsorbent candidate for separation of mixtures containing methane and/or other hydrocarbons.

Conflicts of interest

There are no conflicts to declare.

Acknowledgements

C. J. is indebted to the DFG for funding within the priority program SPP 1928 "COORNET" (grant Ja466/43-1).

Notes and references

‡ HHUD stands for Heinrich-Heine-University Düsseldorf. HHUD-1 and HHUD-2 were reported without the "D" as HHU-1 and HHU-2 in ref. 19 and 45–48.

§ Synthesis of HHUD-3 (short description): a turbid solution prepared by mixing $ZrCl_4$, diamantane-4,9-dicarboxylic acid, formic acid, and DMF (molar ratio 1 : 1.2 : 78 : 1533) was heated at 120 °C for 72 h in a hermetically sealed culture tube. The colourless microcrystalline product was isolated by centrifugation, washed 2× with 5 mL DMF and 2× with 5 mL of EtOH, and dried at 80 °C for 48 h. Yield: 17.1 mg (66%).

¶ Selected crystal data for $C_{75.8}H_{82.1}O_{32.0}Zr_6$ (refined as $[Zr_6O_4(O\{H\})_4(C_{16}H_{18}O_4)_{4.56}(\{H\}COO)_{2.86}]$, {H} not refined), FW = 2052.7, cubic, $Fm\bar{3}m$, a = 23.49022(13) Å, V = 12961.68(12) Å^3, ρ = 1.1048, Z = 4, R_p = 0.0315, wR_p = 0.0450, R_1 = 0.0346, GoF = 5.9. CCDC 2102614 contains the supplementary crystallographic data for this paper.

1 J. Zhou, H. Li, H. Zhang, H. Li, W. Shi and P. Cheng, *Adv. Mater.*, 2015, **27**, 7072–7077.
2 F. A. Almeida Paz, J. Klinowski, S. M. F. Vilela, J. P. C. Tome, J. A. S. Cavaleiro and J. Rocha, *Chem. Soc. Rev.*, 2012, **41**, 1088–1110.
3 I. M. Hönicke, I. Senkovska, V. Bon, I. A. Baburin, N. Bönisch, S. Raschke, J. D. Evans and S. Kaskel, *Angew. Chem., Int. Ed.*, 2018, **57**, 13780–13783.
4 A. U. Czaja, N. Trukhan and U. Muller, *Chem. Soc. Rev.*, 2009, **38**, 1284–1293.
5 P. Kumar, A. Deep and K.-H. Kim, *TrAC, Trends Anal. Chem.*, 2015, **73**, 39–53.
6 T. C. Wang, F. P. Doty, A. I. Benin, J. D. Sugar, W. L. York, E. W. Reinheimer, V. Stavila and M. D. Allendorf, *Chem. Commun.*, 2019, **55**, 4647–4650.
7 U. Schubert, *Coord. Chem. Rev.*, 2022, **469**, 214686.
8 D. Van den Eynden, R. Pokratath and J. De Roo, *Chem. Rev.*, 2022, **122**, 10538–10572.
9 J. H. Cavka, S. Jakobsen, U. Olsbye, N. Guillou, C. Lamberti, S. Bordiga and K. P. Lillerud, *J. Am. Chem. Soc.*, 2008, **130**, 13850–13851.
10 Y. Bai, Y. Dou, L.-H. Xie, W. Rutledge, J.-R. Li and H.-C. Zhou, *Chem. Soc. Rev.*, 2016, **45**, 2327–2367.
11 M. Zhang, Y.-P. Chen, M. Bosch, T. Gentle, K. Wang, D. Feng, Z. U. Wang and H.-C. Zhou, *Angew. Chem.*, 2014, **126**, 834–837.
12 H. Motegi, K. Yano, N. Setoyama, Y. Matsuoka, T. Ohmura and A. Usuki, *J. Porous Mater.*, 2017, **24**, 1327–1333.
13 D. Feng, Z.-Y. Gu, J.-R. Li, H.-L. Jiang, Z. Wie and H.-C. Zhou, *Angew. Chem.*, 2012, **124**, 10453–10456.
14 S. J. Garibay and S. M. Cohen, *Chem. Commun.*, 2010, **46**, 7700–7702.
15 M. Sarker, J. Y. Song and S. H. Jhung, *Chem. Eng. J.*, 2018, **331**, 124–131.
16 J. Winarta, B. Shan, S. M. Mcintyre, L. Ye, C. Wang, J. Liu and B. Mu, *Cryst. Growth Des.*, 2020, **20**, 1347–1362.
17 V. R. Bakuru, S. R. Churipard, S. P. Maradur and S. B. Kalidindi, *Dalton Trans.*, 2019, **48**, 843–847.
18 S. Waitschat, D. Fröhlich and H. Reinsch, *Dalton Trans.*, 2018, **47**, 1062–1070.
19 T. J. Matemb Ma Ntep, H. Reinsch, C. Schlüsener, A. Goldman, H. Breitzke, B. Moll, L. Schmolke, G. Buntkowsky and C. Janiak, *Inorg. Chem.*, 2019, **58**, 10965–10973.
20 J. Lippke, B. Brosent, T. von Zons, E. Virmani, S. Lilienthal, T. Preuße, M. Hülsmann, A. M. Schneider, S. Wuttke, P. Behrens and A. Godt, *Inorg. Chem.*, 2017, **56**, 748–761.
21 J. Perego, S. Bracco, M. Negroni, C. X. Bezuidenhout, G. Prando, P. Carretta, A. Comotti and P. Sozzani, *Nat. Chem.*, 2020, **12**, 845–851.

22 K. B. Idrees, Z. Chen, X. Zhang, M. R. Mian, R. J. Drout, T. Islamoglu and O. K. Farha, *Chem. Mater.*, 2020, **32**, 3776–3782.
23 L. K. Macreadie, E. J. Mensforth, R. Babarao, K. Konstas, S. G. Telfer, C. M. Doherty, J. Tsanaktsidis, S. R. Batten and M. R. Hill, *J. Am. Chem. Soc.*, 2019, **141**, 3828–3832.
24 L. K. Macreadie, R. Babarao, C. J. Setter, S. J. Lee, Omid T. Qazvini, A. J. Seeber, J. Tsanaktsidis, S. G. Telfer, S. R. Batten and M. R. Hill, *Angew. Chem., Int. Ed.*, 2020, **59**, 6090–6098.
25 A. A. Fokin, B. A. Tkachenko, P. A. Gunchenko, D. V. Gusev and P. R. Schreiner, *Chem. – Eur. J.*, 2005, **11**, 7091–7101.
26 H. Schwertfeger, A. A. Fokin and P. R. Schreiner, *Angew. Chem., Int. Ed.*, 2008, **47**, 1022–1036.
27 (*a*) M. A. Gunawan, D. Poinsot, B. Domenichini, P. R. Schreiner, A. A. Fokin and J. C. Hierso, in *Chemistry of organo-hybrids: synthesis and characterization of functional nano-objects*, ed. B. Charleux, C. Copéret and E. Lacôte, Wiley, Hoboken, 2015, p. 69; (*b*) M. A. Gunawan, J.-C. Hierso, D. Poinsot, A. A. Fokin, N. A. Fokina, B. A. Tkachenko and P. R. Schreiner, *New J. Chem.*, 2014, **38**, 28–41.
28 Y. Zhou, A. D. Brittain, D. Kong, M. Xiao, Y. Meng and L. Sun, *J. Mater. Chem. C*, 2015, **3**, 6947–6961.
29 T. Muller and S. Bräse, *RSC Adv.*, 2014, **4**, 6886–6907.
30 A. B. Lysenko, G. A. Senchyk, J. Lincke, D. Lässig, A. A. Fokin, E. D. Butova, P. R. Schreiner, H. Krautscheid and K. V. Domasevitch, *Dalton Trans.*, 2010, **39**, 4223–4231.
31 M. J. Cliffe, W. Wan, X. Zou, P. A. Chater, A. K. Kleppe, M. G. Tucker, H. Wilhelm, N. P. Funnell, F.-X. Coudert and A. L. Goodwin, *Nat. Commun.*, 2014, **5**, 4176.
32 M. Ermer, J. Mehler, M. Kriesten, Y. S. Avadhut, P. S. Schulz and M. Hartmann, *Dalton Trans.*, 2018, **47**, 14426–14430.
33 M. J. Katz, Z. J. Brown, Y. J. Colón, P. W. Siu, K. A. Scheidt, R. Q. Snurr, J. T. Hupp and O. K. Farha, *Chem. Commun.*, 2013, **49**, 9449–9451.
34 G. C. Shearer, S. Chavan, S. Bordiga, S. Svelle, U. Olsbye and K. P. Lillerud, *Chem. Mater.*, 2016, **28**, 3749–3761.
35 O. V. Gutov, M. González Hevia, E. C. Escudero-Adán and A. Shafir, *Inorg. Chem.*, 2015, **54**, 8396–8400.
36 G. C. Shearer, S. Chavan, J. Ethiraj, J. G. Vitillo, S. Svelle, U. Olsbye, C. Lamberti, S. Bordiga and K. P. Lillerud, *Chem. Mater.*, 2014, **26**, 4068–4071.
37 Y. Huang, W. Qin, Z. Li and Y. Li, *Dalton Trans.*, 2012, **41**, 9283–9285.
38 M. Thommes, K. Kaneko, A. V. Neimark, J. P. Olivier, F. Rodriguez-Reinoso, J. Rouquerol and K. S. W. Sing, *Pure Appl. Chem.*, 2015, **87**, 1051–1069.
39 L. Y. Molefe, N. M. Musyoka, J. Ren, H. W. Langmi, M. Mathe and P. G. Ndungu, *J. Inorg. Organomet. Polym. Mater.*, 2021, **31**, 80–88.
40 D. H. Hong and M. P. Suh, *Chem. – Eur. J.*, 2014, **20**, 426–434.
41 E. Poirier, R. Chahine and T. K. Bose, *Int. J. Hydrogen Energy*, 2001, **26**, 831–835.
42 P. Bénard and R. Chahine, *Scr. Mater.*, 2007, **56**, 803–808.
43 J. P. Wagner and P. R. Schreiner, *Angew. Chem., Int. Ed.*, 2015, **54**, 12274–12296.
44 D. Danovich, S. Shaik, F. Neese, J. Echeverría, G. Aullón and S. Alvarez, *J. Chem. Theory Comput.*, 2013, **9**, 1977–1991.
45 T. J. Matemb Ma Ntep, H. Reinsch, B. Moll, E. Hastürk, S. Gökpinar, H. Breitzke, C. Schlüsener, L. Schmolke, G. Buntkowsky and C. Janiak, *Chem. – Eur. J.*, 2018, **24**, 14048–14053.
46 T. J. Matemb Ma Ntep, H. Reinsch, J. Liang and C. Janiak, *Dalton Trans.*, 2019, **48**, 15849–15855.
47 T. J. Matemb Ma Ntep, H. Breitzke, L. Schmolke, C. Schlüsener, B. Moll, S. Millan, N. Tannert, I. El Aita, G. Buntkowsky and C. Janiak, *Chem. Mater.*, 2019, **31**, 8629–8638.
48 T. J. Matemb Ma Ntep, V. K. Gramm, U. Ruschewitz and C. Janiak, *Chem. Commun.*, 2022, **58**, 8900–8933.

